Activation of O_2, CO, and CO_2 by Pt^+: The Thermochemistry of PtO^+

Xiao-Guang Zhang and P. B. Armentrout*

Department of Chemistry, University of Utah, Salt Lake City, Utah 84112-0850

Received: July 12, 2003; In Final Form: August 22, 2003

Reactions of Pt^+ with O_2, CO, and CO_2 have been studied as a function of kinetic energy using guided ion beam tandem mass spectrometry in order to elucidate the bond energy of the PtO^+ product. To further characterize the reaction of Pt^+ with CO_2, the reverse reaction of PtO^+ with CO, and the collision-induced dissociation of $PtCO_2^+$ with Xe and Ar are also studied. In all cases, the kinetic energy dependences for these reactions show endothermic behavior except for $PtO^+ + CO \rightarrow Pt^+ + CO_2$ and $PtCO_2^+ + Xe \rightarrow PtXe^+ + CO_2$. Analyses of the endothermic reaction cross sections yield the 0 K bond dissociation energies (BDEs) in eV (kJ/mol) of $D_0(Pt^+-O) = 3.26 \pm 0.07$ (315 ± 7), $D_0(Pt^+-CO) = 2.28 \pm 0.05$ (220 ± 5), $D_0(Pt^+-CO_2) = 0.62 \pm 0.05$ (60 ± 5), and $D_0(Pt^+-C) = 5.46 \pm 0.05$ (527 ± 5), reasonably consistent with available theoretical values. Combining the PtO^+ BDE measured here with literature data also yields the ionization energy of PtO as 9.52 ± 0.25 eV. These data, along with ab initio calculations at the B3LYP/6-311+G(3df) level, enable the potential energy surfaces for the activation of CO_2 by Pt^+ to be mapped out in some detail. Evidence that $PtCO_2^+$ has stable forms of both $O-Pt^+-CO$ and $Pt^+ \cdot CO_2$ are presented.

1. Introduction

Platinum is one of the most versatile and all-purpose metal catalysts.[1,2] In particular, it is an active component of catalysts for the oxidation of CO and unburned hydrocarbons in the control of car emissions.[1] Insight into the interaction of platinum metal and its oxides with O_2, CO, and CO_2 can be obtained by examining analogous reactions in the gas phase using a guided ion beam tandem mass spectrometer. The gas phase is an ideal arena for detailed study of the energetics of bond-making and bond-breaking processes at a molecular level. Because metal supports and interactions are absent, quantitative thermodynamic and intrinsic mechanistic information for various bond activation processes can be obtained. Such insight may be useful in better understanding and improving the use of platinum and its oxides to convert CO and unburned hydrocarbons in the presence of O_2 into nontoxic and nonpolluting chemicals.

Previously we have used guided ion beam tandem mass spectrometry to systematically study the metal monoxide cations, MO^+, of the first-row[3−11] and second-row[5,9,12−17] transition metals, and other metals.[9,18−20] In the present work, we extend these studies to the third-row transition metal ion, platinum. Recently Schwarz's group used ion cyclotron resonance (ICR) mass spectrometry, various theoretical calculations, and preliminary experimental values from our work as anchors to study the energetics and reactivities of PtO^+ and PtO_2^+ species.[21−24] Because the ICR experiments were performed at thermal energy, they cannot supply complete and quantitative information about the potential energy surfaces for the activation of O_2, CO, and CO_2 by Pt^+. Using guided ion beam tandem mass spectrometry, we can examine the kinetic energy dependences of both exothermic and endothermic processes. Analyses of such data provide experimental BDEs that can be used as benchmarks for comparison with theoretical models of the structure and bonding of PtO^+. Furthermore, PtO^+ has been shown to activate and oxygenate hydrocarbons,[21−25] making it a potentially useful model of systems that can transform hydrocarbons into other useful chemicals. The present work provides thermodynamic, dynamic, and mechanistic information for the activation of O_2, CO, and CO_2 by Pt^+. In addition, this study is part of ongoing efforts in our laboratory to understand the periodic trends in the BDEs of metal oxides.[3−17,26−28]

2. Experimental Section

2.1. General Procedures. The guided ion beam tandem mass spectrometer on which these experiments were performed has been described in detail previously.[29,30] Briefly, Pt^+, PtO^+, and $PtCO_2^+$ ions are generated in a direct current discharge flow tube source described below, extracted from the source, accelerated, and focused into a magnetic sector momentum analyzer for mass selection of primary ions. The mass-selected ions are then decelerated to a desired kinetic energy and focused into an octopole ion beam guide that uses radio frequency electric fields to trap the ions in the radial direction and ensure complete collection of reactant and product ions.[31,32] The octopole passes through a static gas cell with an effective length of 8.26 cm that contains the reaction partner at a low pressure (usually less than ~0.3 mTorr) so that multiple ion−molecule collisions are improbable. All results reported here result from single bimolecular encounters, as verified by pressure-dependence studies. The unreacted parent and product ions are confined radially in the guide until they drift to the end of the octopole, where they are extracted, focused, and passed through a quadrupole mass filter for mass analysis of products. Ions are subsequently detected with a secondary electron scintillation ion detector using standard pulse-counting techniques. Reaction cross sections are calculated from product ion intensities relative to reactant ion intensities after correcting for background signals.[33] Uncertainties in the absolute cross sections are estimated to be ±20%.

The kinetic energy of the ions is varied in the laboratory frame by scanning the dc bias on the octopole rods with respect to the potential of the ion source region. Laboratory (lab) ion

* Corresponding author. E-mail: armentrout@chem.utah.edu.

10.1021/jp036014j CCC: $25.00
Published on Web 09/30/2003

energies are converted to energies in the center-of-mass frame (CM) by using the formula $E_{CM} = E_{lab}m/(m + M)$, where m and M are the neutral and ionic reactant masses, respectively. Two effects broaden the cross section data: the kinetic energy distribution of the reactant ion and thermal motion of the neutral reactant gas (Doppler broadening).[34] The absolute zero and the full width at half-maximum (fwhm) of the kinetic energy distribution of the reactant ions are determined using the octopole beam guide as a retarding potential analyzer, as described previously.[33] The distributions of ion energies, which are independent of energy, are nearly Gaussian and have typical fwhm of 0.3−1.0 eV (lab) in these studies. Uncertainties in the absolute energy scale are ± 0.05 eV (lab).

2.2. Ion Source. Pt^+ ions are produced in a direct current discharge flow tube (DC/FT) source,[30] consisting of a cathode held at high negative voltage (0.7−1.3 kV) over which a flow of approximately 90% He and 10% Ar passes at a total pressure of 0.3−0.4 Torr and ambient temperature. In this work, the cathode is platinum foil attached to an iron holder. Ar^+ ions created in the discharge are accelerated toward the platinum cathode, thereby sputtering Pt^+. Pt^+ ions are then swept down a one-meter long flow tube. The ions undergo $\sim 10^5$ thermalizing collisions with He and $\sim 10^4$ collisions with Ar before entering the guided ion beam apparatus. Generally, these conditions are sufficient to produce atomic ions in their ground electronic state. However, trace amounts of low-lying excited states of Pt^+ are observed to survive these flow conditions, as found by examining the reactions of Pt^+ with O_2 and CO_2, described in detail below. These excited species are easily removed by introducing O_2 or N_2O to the flow tube about 30 cm downstream of the discharge zone at a pressure of ~20 mTorr.

With the addition of such cooling gases, the DC/FT source produces metal ions in the ground electronic state. Therefore, Pt^+ ions created under such conditions are believed to be in the ground $^2D(5d^9)$ electronic state term and largely in the $^2D_{5/2}$ lowest spin−orbit level. As discussed in detail elsewhere,[35,36] a conservative estimate of the state populations is >99.7% $^2D_{5/2}$ and <0.3% $^4F_{9/2}$, such that the average electronic energy is calculated to be ≤0.002 eV for Pt^+. This estimated population is consistent with the failure to observe any evidence for electronically excited Pt^+ species in the present and related studies,[35−37] once the cooling gas (O_2 or N_2O) is added to the flow tube.

PtO^+ ions are produced through reaction of Pt^+ with N_2O, and $PtCO_2^+$ ions are produced by the three-body condensation of Pt^+ with CO_2 in the DC/FT source. In those cases, the reactant gas (N_2O or CO_2) is introduced into the flow tube 30 cm downstream of the discharge zone at a pressure of ~2 mTorr. These ions undergo $\sim 10^5$ thermalizing collisions with He and $\sim 10^4$ collisions with Ar along the flow tube before entering the guided ion beam apparatus. These collisions with the He/Ar flow gas stabilize and thermalize the ions both rotationally and vibrationally. In general, we assume that these ions are in their ground electronic state and that the internal energy of these molecular ions is well described by a Maxwell−Boltzmann distribution of rotational and vibrational states corresponding to 300 K, the temperature of the flow tube. Previous studies from this laboratory have shown that these assumptions are consistent with the production of thermalized molecular ions under similar conditions.[26−28,35,38,39] As detailed below, there are indications for the possibility of small amounts of electronically excited states in the PtO^+ beam produced here.

2.3. Data Analysis. The kinetic-energy dependence of product cross sections is analyzed to determine E_0, the energy threshold for product formation at 0 K. E_0 differs from the apparent threshold observed under laboratory conditions because of the kinetic and internal energy distributions of the reactants. Each of those contributions allows reactions to occur at energies below E_0. To determine E_0, endothermic reaction cross sections are modeled using eq 1,[39−42]

$$\sigma(E) = \sigma_0 \sum g_i (E + E_{el} + E_i - E_0)^n / E \qquad (1)$$

where σ_0 is an energy-independent scaling factor, E is the relative kinetic energy of the reactants, E_{el} is the electronic energy of the metal cation (when Pt^+ is the reactant ion), and n is an adjustable parameter that characterizes the energy dependence of the process.[43] The sum considers contributions from rovibrational states of the reactants at 300 K, denoted by i, having energies E_i and populations g_i, where $\sum g_i = 1$. As noted above, E_{el} is believed to be ≤0.002 eV for Pt^+. The various sets of vibrational frequencies and rotational constants used to determine E_i in this work are taken from the literature for O_2,[44] CO,[44] CO_2,[45] and PtO^+.[24,46] The molecular constants for $PtCO_2^+$ are taken from the calculations detailed below. Before comparison with the experimental data, eq 1 is convoluted with the kinetic energy distributions of the reactant ions and neutral reactants at 300 K. The σ_0, n, and E_0 parameters are then optimized using a nonlinear least-squares analysis to give the best reproduction of the data.[33] Error limits for E_0 are calculated from the range of threshold values for different data sets over a range of acceptable n values (as specified in the Table of fitting parameters given below) combined with the absolute errors in the kinetic energy scale and internal energies of reactant ions.

At higher energies, the cross sections decline because the product ions have sufficient energy to dissociate. In this high-energy region, the data can be modeled by modifying eq 1 to include the dissociation probability according to a statistical model discussed elsewhere.[18] This probability is controlled by two parameters: p, which is an adjustable parameter similar to n, and E_d, which is the energy at which product ions start decomposing. In this study, the values of p and E_d are allowed to vary (although p can only hold integral values) and are used to fit cross sections of Pt^+ with O_2 and CO, PtO^+ with CO, and $PtCO_2^+$ with Ar. Use of this high-energy model does not alter significantly the analysis of the threshold regions.

2.4. Theoretical Calculations. To establish the character of the molecular orbitals of PtO^+ and to examine the potential energy surface of the $PtCO_2^+$ system, quantum chemistry calculations were computed with the B3LYP hybrid density functional method[47,48] and performed with the GAUSSIAN 98 suite of programs.[49] The B3LYP functional is based on the hybrid gradient-corrected exchange functional proposed by Becke[49] combined with the gradient-corrected correlation functional of Lee, Yang and Parr.[50] The 60 core electrons of platinum are described using a basis set for Pt described by Ohanessian et al.,[50] which is based on the relativistic effective core potentials (ECP) of Hay-Wadt (HW),[51] equivalent to the Los Alamos ECP (LANL2DZ) basis set. Whereas the HW-ECP is optimized for neutral atoms, the altered basis set of Ohanessian et al. (HW+) accounts for differential contraction of the s orbitals compared to the d orbitals induced by the positive charge. In previous work,[35] we also performed calculations using an expanded HW-ECP basis set in which one s, one p, and one d function were uncontracted, one diffuse d function and two f functions were added, and the s orbitals were contracted (HW+X).[23] Calculations of potential energy surfaces (relaxed potential energy scans) were conducted using a 6-31+G(2d)

basis set for carbon and oxygen, whereas the triple-ζ basis, 6-311+G(3df), was used to characterize all stationary points on these potential energy surfaces. Frequency calculations at the triple-ζ level verified the character of all stationary points. In all cases, the thermochemistry calculated here is corrected for zero-point energies after scaling the vibrational frequencies by 0.9804.[52] As a point of comparison, the single-point bond energies for O−O, C−O, and O−CO are calculated as 5.279, 11.059, and 5.529 eV (uncorrected for spin−orbit coupling) compared to the experimental values of 5.115,[44] 11.108,[44] and 5.453 eV,[53] respectively.

3. Experimental Results

3.1. Electronic States of Pt^+. Figure 1 shows cross sections for reaction of Pt^+ with O_2. Two ionic products are formed in reactions 2 and 3 when no cooling gas is added into the FT

$$Pt^+ + O_2 \rightarrow PtO^+ + O \quad (2)$$

$$\rightarrow Pt + O_2^+ \quad (3)$$

source (open symbols). The cross section for reaction 2 shows inefficient exothermic reactivity at the lowest energies and a strong endothermic feature beginning about 1.5 eV. Compared to the Langevin-Gioumousis-Stevenson (LGS) model for collisions between ion and neutral molecules,[54] which has an $E^{-0.5}$ energy dependence, the exothermic reactivity observed here is 1800 ± 100 times smaller at thermal energies (~0.04 eV). When O_2 or N_2O is added into the FT source (closed symbols), the exothermic feature disappears and the charge transfer reaction 3 is eliminated. Clearly these reactions result from excited states of Pt^+ (which could have populations as small as 0.06% = 100%/1800), which are removed by reaction with O_2 or N_2O in the FT source. Therefore, we assume that Pt^+ ions after quenching are in their ground electronic state, $^2D(5d^9)$. Given the ionization energies of 12.07 eV for O_2[55] and 8.96 eV for Pt,[56] the energy dependence of the charge-transfer reaction 3 indicates that excited states above about 3.1 eV may be populated in the primary beam of Pt^+ when no quenching gas (O_2 or N_2O) is introduced into the DC/FT source. The cross section for O_2^+ declines sharply above about 2 eV. This is because the relative voltages on the octopole and quadrupole prevent these slow moving ions from being transmitted efficiently at higher energies.

Pt^+ reacts with CO_2 to form three ionic products in reactions 4, 5, and 6

$$Pt^+ + CO_2 \rightarrow PtO^+ + CO \quad (4)$$

$$\rightarrow PtCO^+ + O \quad (5)$$

$$\rightarrow Pt + CO_2^+ \quad (6)$$

when no quenching gases are introduced into the DC/FT source. The data are shown in the Supporting Information. Compared to the LGS collision cross section,[54] the total exothermic reactivity observed is $3 \pm 1 \times 10^3$ times smaller at thermal energies. The charge-transfer product CO_2^+ is no longer observed after O_2 or N_2O is introduced into the FT source, as are the very small exothermic features in the cross sections for PtO^+ and $PtCO^+$. Clearly, formation of CO_2^+ and the exothermic features result from reactions of excited states of Pt^+ with CO_2, which could have populations as small as 0.03%. Given the ionization energies of 13.78 eV for CO_2[57] and 8.96 eV for Pt,[56] the nearly thermoneutral charge-transfer reaction 6 implies that there are excited states near 4.8 eV in the primary beam of Pt^+ when no quenching gas is introduced into the DC/FT source. The CO_2^+ cross section declines rapidly above about 3 eV, again because the relative voltage settings on the octopole and quadrupole do not transmit these products at higher energies.

When no cooling gas (O_2 or N_2O) is used, a CO^+ charge-transfer product is observed in trace amounts from reactions of excited states of Pt^+ with CO. This product disappears when a cooling gas is used in the flow tube source. Because the ionization energies of CO and Pt are 14.01 eV[58] and 8.96 eV,[56] respectively, the observation of CO^+ indicates that there are excited states of Pt^+ above 5.05 eV in the primary beam when no quenching gas is introduced into the DC/FT source.

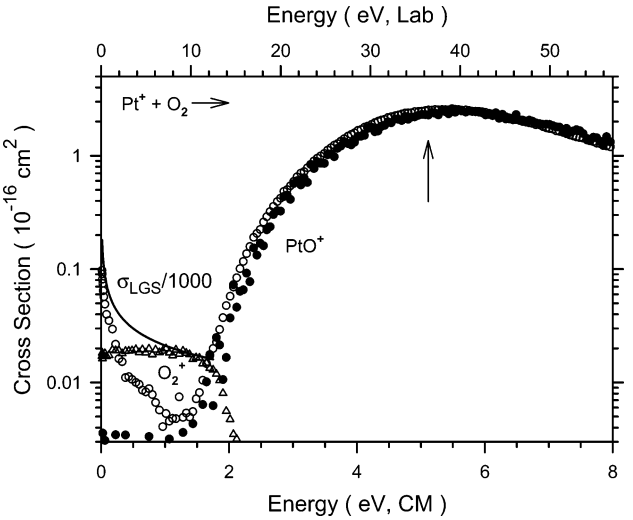

Figure 1. Cross sections for reaction of Pt^+ with O_2 as a function of kinetic energy in the center-of-mass frame (lower axis) and laboratory frame (upper axis). The data are shown for Pt^+ ions generated with ~20 mTorr O_2 introduced into the flow tube (solid circles) and without O_2 introduced into the flow tube (open circles and triangles). The line shows the Langevin-Gioumousis-Stevenson (LGS) collision cross section divided by 1000. The arrow indicates D_0(O−O) at 5.12 eV.

TABLE 1: Bond Dissociation Energies at 0 K

	bond energy (eV)[a]		
		theory	
bond	experiment	literature	this work
O−O	5.115 ± 0.002[b]		5.279
C−O	11.108 ± 0.005[b]		11.059
OC−O	5.453 ± 0.002[c]		5.529
Pt^+−O	3.26 ± 0.07, 2.9 ± 0.4,[d] 3.164[e]	3.09,[f,g] 2.96,[f,g] 2.95,[f,g] 2.92[f,g]	2.78[g]
Pt^+−C	5.46 ± 0.05, 5.43 ± 0.05[h]	5.52,[g,h] 5.43,[g,h] 5.57[g,h]	
Pt^+−CO	2.26 ± 0.09, 2.20 ± 0.05[i]	2.33[i]	2.27[g]
Pt^+−CO_2	0.62 ± 0.05		0.56[g]
OPt^+−CO	2.21 ± 0.10		1.90

[a] From this work, except as noted. [b] Reference 44. [c] Reference 59. [d] Reference 64. [e] Reference 62. [f] Reference 24. [g] Values have been adjusted by 0.418 eV for the Pt^+ spin−orbit asymptote. See text. [h] Reference 35. [i] Reference 38.

3.2. Reaction of $Pt^+(^2D)$ with O_2. Figure 2 shows the cross section for reaction 2 as a function of kinetic energy after excited states of Pt^+ are quenched. The reaction cross section rises from an apparent threshold of ~1.5 eV and reaches a maximum at the dissociation energy of O_2, 5.12 eV (Table 1). Above this energy, PtO^+ may be formed with an internal energy in excess

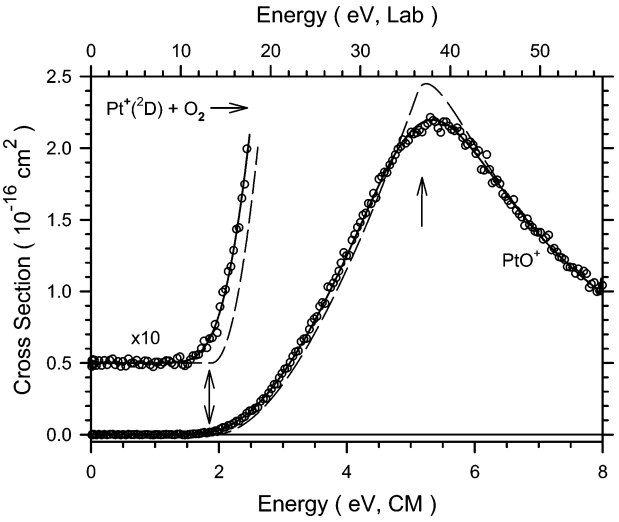

Figure 2. Cross sections for reaction of $Pt^+(^2D)$ with O_2 as a function of kinetic energy in the center-of-mass frame (lower axis) and laboratory frame (upper axis). Pt^+ ions are produced with ~20 mTorr O_2 introduced into the flow tube. The best fit to the data using eq 1 with parameters in Table 2 is shown as a dashed line. The solid line shows this model convoluted over the kinetic and internal energy distributions of the neutral reactant and ion. The arrows indicate the threshold energy E_0 and $D_0(O-O)$ at 5.12 eV.

of its bond dissociation energy and therefore begins to dissociate in the overall reaction 7.

$$Pt^+ + O_2 \rightarrow PtO^+ + O \rightarrow Pt^+ + O + O \qquad (7)$$

The cross section data for reaction 2 are analyzed using eq 1, and the fitting parameters obtained are listed in Table 2. The threshold model of eq 1 reproduces the experimental data nicely up to ~4.5 eV. To accurately reproduce the data above this energy, the modification of eq 1 that includes the dissociation process must be used.[18] With this modified model, the PtO^+ cross section is reproduced well up to 8 eV with $p = 3$ and E_d set to the literature value for $D_0(O-O) = 5.12$ eV as shown in Figure 2.

3.3. Reactions of $Pt^+(^2D)$ with CO. Pt^+ reacts with CO to form two ionic products in reactions 8 and 9.

$$Pt^+ + CO \rightarrow PtC^+ + O \qquad (8)$$

$$\rightarrow PtO^+ + C \qquad (9)$$

Figure 3 shows the cross sections as a function of kinetic energy after excited states of Pt^+ are quenched with the addition of O_2 at ~20 mTorr into the FT source. Both reactions 8 and 9 are endothermic. Platinum carbide ion is the main product ion and its cross section begins to decline because of the competition with reaction 9. The PtO^+ channel declines because of the overall reaction 10, dissociation of the PtO^+ product,

$$Pt^+ + CO \rightarrow PtO^+ + C \rightarrow Pt^+ + O + C \qquad (10)$$

which has a thermodynamic threshold of $D_0(C-O) = 11.11$ eV (Table 1). The cross section data are analyzed using eq 1 and the fitting parameters obtained are listed in Table 2. The model reproduces the experimental data of the PtC^+ product up to ~8 eV, the total cross section up to ~10 eV, and the PtO^+ product up to 15 eV with $p = 4$ and $E_d = 11.11$ eV as shown in Figure 3.

TABLE 2: Parameters of Eq 1 Used in Modeling Various Reaction Systems

reactants	products	σ_0	n	E_0 (eV)
$Pt^+ + O_2$	$PtO^+ + O$	0.7 ± 0.1	2.3 ± 0.1	1.85 ± 0.05
$Pt^+ + CO$	$PtC^+ + O$	0.6 ± 0.1	1.3 ± 0.1	5.56 ± 0.05
	$PtO^+ + C$	0.3 ± 0.1	1.7 ± 0.1	7.84 ± 0.05
$Pt^+ + CO_2$	$PtO^+ + CO$	0.6 ± 0.1	1.7 ± 0.1	2.19 ± 0.08
	$PtO^+ + PtCO^+$ [a]	0.5 ± 0.1	2.2 ± 0.1	2.19 ± 0.05
	$PtCO^+ + O$	1.2 ± 0.3	1.9 ± 0.1	3.17 ± 0.05
$PtO^+ + CO$	$PtCO^+ + O$ [b]	0.05 ± 0.02	1.0	0.35 ± 0.05
	$PtCO^+ + O$ [b]	0.10 ± 0.03	1.8 ± 0.1	1.08 ± 0.10
$PtCO_2^+ + Xe$	$Pt^+ + CO_2 + Xe$	16.6 ± 1.0	1.7 ± 0.1	0.76 ± 0.05
$PtCO_2^+ + Ar$	$Pt^+ + CO_2 + Ar$	7.2 ± 0.1	1.3 ± 0.1	0.62 ± 0.05
	$PtAr^+ + CO_2$	4.4 ± 0.3	1.7 ± 0.2	0.32 ± 0.05

[a] Total cross section of $PtO^+ + CO$ and $PtCO^+ + O$ processes were modeled. [b] Modeling of this cross section is described in detail in the text. The model with the lower energy threshold was obtained by holding $n = 1.0$.

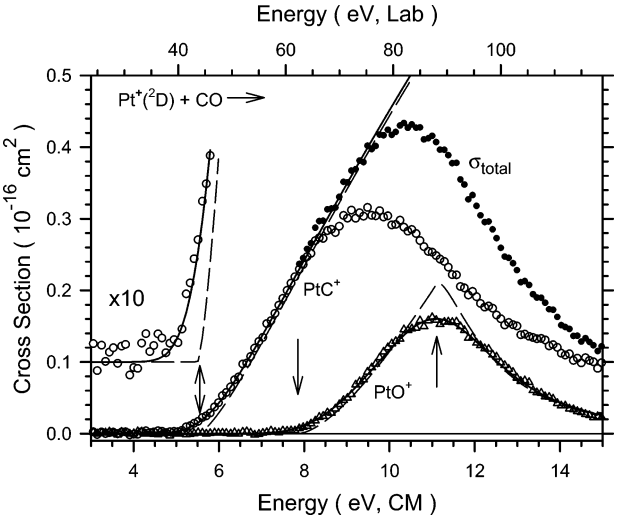

Figure 3. Cross sections for reaction of $Pt^+(^2D)$ with CO as a function of kinetic energy in the center-of-mass frame (lower axis) and laboratory frame (upper axis). Pt^+ ions are produced with ~20 mTorr O_2 introduced into the flow tube. Small circles show the total cross sections. The best fits to the data using eq 1 with parameters in Table 2 are shown as dashed lines. The solid lines show this model convoluted over the kinetic and internal energy distributions of the neutral reactant and ion. The arrows indicate the threshold energies E_0 and $D_0(C-O)$ at 11.11 eV.

3.4. Reactions of $Pt^+(^2D)$ with CO_2. Figure 4 shows the cross sections as a function of kinetic energy for reactions 4 and 5 when $Pt^+(^2D_{5/2})$ is produced in the FT source by the addition of N_2O at ~20 mTorr. The reactions exhibit typical endothermic behavior in which the cross sections rise from apparent thresholds and reach maxima near the dissociation energy of OC−O, 5.45 eV (Table 1). Above this energy, PtO^+ and $PtCO^+$ may be formed with internal energies in excess of their bond dissociation energies. Therefore, these products begin to dissociate in the overall reaction 11.

$$Pt^+ + CO_2 \rightarrow Pt^+ + CO + O \qquad (11)$$

The cross section data are analyzed using eq 1, and the fitting parameters obtained are listed in Table 2. The model reproduces the experimental data of the $PtCO^+$ product and the total cross sections up to ~5.5 eV. For the PtO^+ cross section, the model reproduces the data well only up to ~3 eV, because the shape of this cross section is influenced by competition with $PtCO^+$ formation above this energy.

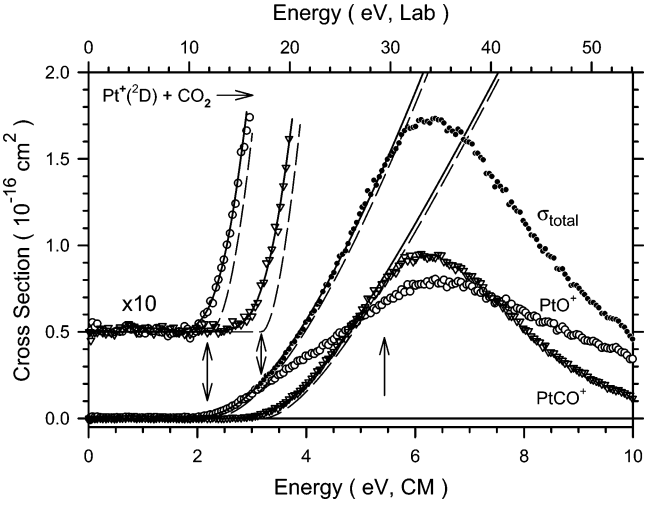

Figure 4. Cross sections for reaction of $Pt^+(^2D)$ with CO_2 as a function of kinetic energy in the center-of-mass frame (lower axis) and laboratory frame (upper axis). Pt^+ ions are produced with ~20 mTorr N_2O introduced into the flow tube. Small circles show the total cross sections. The best fits to the data using eq 1 with parameters in Table 2 are shown as dashed lines. The solid lines show this model convoluted over the kinetic and internal energy distributions of the neutral reactant and ion. The arrows indicate the threshold energies E_0 and $D_0(OC-O)$ at 5.45 eV.

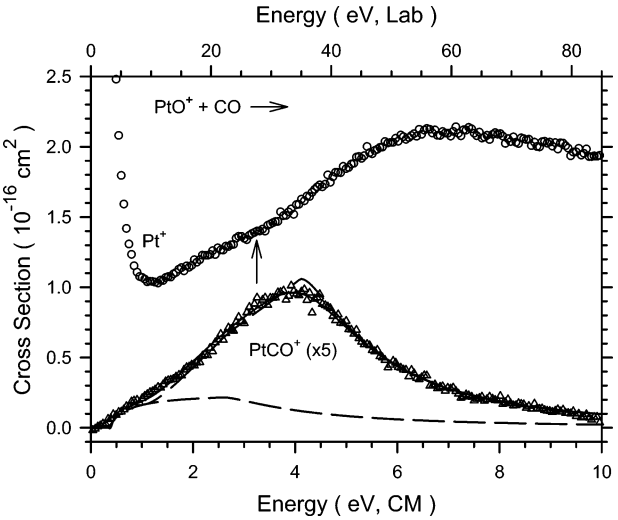

Figure 5. Cross sections for reactions of PtO^+ with CO as a function of kinetic energy in the center-of-mass frame (lower axis) and laboratory frame (upper axis). The best fits to the $PtCO^+$ data using eq 1 with the two sets of parameters in Table 2 are shown as dashed lines. The solid line shows this model convoluted over the kinetic and internal energy distributions of the neutral reactant and ion. The arrow indicates $D_0(Pt^+-O)$ at 3.26 eV.

3.5. Reactions of PtO^+ with CO. PtO^+ reacts with CO to form two ionic products in reactions 12, 13, and 14 as shown in Figure 5.

$$PtO^+ + CO \rightarrow Pt^+ + CO_2 \quad (12)$$

$$\rightarrow Pt^+ + O + CO \quad (13)$$

$$\rightarrow PtCO^+ + O \quad (14)$$

For production of Pt^+, there are three features. The exothermic reaction observed at the lowest energies must correspond to reaction 12 and is consistent with previous observations of this process at thermal energies in ICR studies.[24] There is an endothermic feature that begins near 1 eV, and evidence for another, which becomes obvious slightly above 3.26 eV, the energy expected for reaction 13, the simple collision-induced dissociation of PtO^+ (see below). One possible explanation for two features corresponding to formation of $Pt^+ + CO_2$ are spin-forbidden and spin-allowed pathways, a hypothesis discussed in more detail below. Production of $PtCO^+$ in the ligand exchange reaction 14 is endothermic and also has two features. Because of the complex shape of this cross section, the analysis using eq 1 is less certain. Reasonable fitting parameters in eq 1 needed to reproduce the cross section data for $PtCO^+$ are listed in Table 2 and the model is shown in Figure 5. This model includes dissociation at high energy using parameters $p = 1$ and $E_d = 3.26 - 0.65 = 2.61$ eV (where 0.65 eV is the excitation energy of PtO^+ determined below), the onset for formation of $Pt^+ + O + CO$, and $p = 3$ and $E_d = 4.1$ eV.

The cross section for reaction 12 decreases with increasing energy, indicating an exothermic reaction having no barrier in excess of the energy asymptote of the reactants. Compared to the LGS collision cross section,[54] which has an $E^{-0.5}$ energy dependence, we find that this reaction cross section declines approximately as $E^{-0.6\pm0.1}$ below 0.1 eV and as $E^{-1.7\pm0.1}$ from 0.15 to 0.7 eV. For comparison to the literature, our cross sections can be converted to a rate constant by using the expression, $k(\langle E\rangle) = v\,\sigma(E)$ where the velocity is $v = (2E/\mu)^{1/2}$ and $\mu = mM/(m + M)$ is the reduced mass of the reactants. The rate constant depends on the mean energy of the reactants, which includes the average thermal motion of the neutral, such that $\langle E\rangle = E + (3/2)\gamma k_B T$ where $\gamma = M/(m + M)$. For the reaction of PtO^+ with CO, we obtain $k = 3.5 \pm 0.7 \times 10^{-10}$ $cm^3\ s^{-1}$ at 300 K. This value compares favorably with the literature rate constant obtained by ICR mass spectrometry of 6.4×10^{-10} $cm^3\ s^{-1}$.[24] Compared to the LGS collision rate, $k_{LGS} = 5.9 \times 10^{-10}$ $cm^3\ s^{-1}$, we find that the reaction of PtO^+ with CO occurs with an efficiency of 60 ± 12% at the lowest energies.

3.6. Collision-Induced Dissociation of $PtCO_2^+$ with Xe and Ar. Cross sections for the interaction of a rare gas, Xe or Ar, with $PtCO_2^+$ formed by three-body condensation of Pt^+ with CO_2 in the DC/FT source are given in supporting material. The products observed correspond to reactions 15 and 16.

$$PtCO_2^+ + Rg \rightarrow Pt^+ + CO_2 + Rg \quad (15)$$

$$\rightarrow PtRg^+ + CO_2 \quad (16)$$

For the Xe system, the ligand exchange reaction 16 is exothermic, indicating that the BDE of $PtXe^+$ is higher than that of Pt^+-CO_2. For the Xe system, the exothermic ligand exchange reaction 16 reaches a reaction efficiency of 56 ± 11% at the lowest energies in comparison with the LGS collision rate.[54] Thus, the shape of the Pt^+ cross section for reaction 15 may be strongly influenced by competition with the ligand exchange process.[59,60] For the Ar system, the smaller BDE for Pt^+-Ar makes the ligand exchange reaction 16 endothermic. The cross section data for the two systems are analyzed using eq 1 and the fitting parameters obtained are listed in Table 2. The models are shown in the supporting material. For the Ar system where the ligand exchange reaction 16 is endothermic, the model of eq 1 reproduces this cross section up to 3 eV with $p = 1$ and $E_d = 0.86$ eV.

4. Thermochemical Results

The endothermic cross sections in each reaction system are analyzed in detail using eq 1 as described above. The optimum values of parameters of eq 1 are listed for each system in Table 2. Because the rotational, vibrational, and translational energy distributions of reactants are explicitly included in the modeling, the E_0 thresholds determined using eq 1 correspond to 0 K. From the thresholds measured, the BDEs at 0 K for the platinum−ligand product ions observed in the reaction of $Pt^+ + L-R$ to form $PtL^+ + R$ can be calculated using eq 17

$$D_0(Pt^+ - L) = D_0(L - R) - E_0 \qquad (17)$$

where the $D_0(L-R)$ values needed are given in Table 1. For collision-induced dissociation (CID), the threshold measured can correspond directly to the BDE for the broken bond. For both bimolecular reactions and CID, we assume that there are no activation barriers in excess of the endothermicity of the reaction, an assumption that is often true for ion−molecule reactions because of the strong long-range attractive forces.[26,39,41,61]

4.1. Pt^+-O. PtO^+ is observed in the reactions of Pt^+ with O_2, CO, and CO_2. The bond dissociation energies for $D_0(Pt^+-O)$ determined in the three reactions are 3.26 ± 0.05, 3.27 ± 0.05, and 3.26 ± 0.08 eV, respectively. Our best value for the bond energy of Pt^+-O is the weighted average of all three values: 3.26 ± 0.07 eV (where the uncertainty is two standard deviations of the mean). This bond energy agrees with the value of 3.164 eV obtained in a recent photodissociation experiment[62] and with the preliminary value from the present work cited elsewhere.[23] It is also within experimental error of the value of 2.9 ± 0.4 eV obtained by combining data on PtO from Knudsen cell mass spectrometry experiments[63,64] with an electron ionization energy of 10.1 ± 0.3 eV from the same study.

Theoretical calculations show that the ground state of PtO^+ is $^4\Sigma^-$ with a valence electron configuration of $1\sigma^2 2\sigma^2 1\pi^4 1\delta^4 2\pi^2 3\sigma^1$.[22] To establish the character of these orbitals, we performed calculations as described above. These show that the 1σ is largely O(2s), with the 2σ and 1π being bonding orbitals, the 2π and unoccupied 4σ being antibonding orbitals, the 1δ are pure metal 5d nonbonding orbitals, and the 3σ is largely Pt(6s) although this orbital also has O(2pσ) and Pt(5dσ) character. Thus, PtO^+ has a strong σ bond ($2\sigma^2$)and two-half π bonds ($1\pi^4 2\pi^2$) because of the single occupancy of the 2π antibonding orbitals. There is also a low-lying $^2\Sigma^-$ state having the same electronic configuration, which we calculate lies 0.27 eV higher in energy, whereas the more sophisticated calculations of Heinemann et al.[22] find an excitation energy of 0.51 eV. Indeed these calculations find a manifold of excited states: $^2\Pi$, 0.83 eV; $^2\Delta$, 0.92 eV; $^4\Delta$, 1.08 eV; $^2\Sigma^+$, 1.22 eV; $^2\Pi$, 1.24 eV; $^2\Delta$, 1.60 eV; and $^4\Pi$, 1.80 eV.

Next we compare our experimental BDE to theoretical calculations in the literature. In making this comparison, it is important to note that the experimental value is referenced to the energy of the Pt^+ ($^2D_{5/2}$) ground state at 0.0 eV. In contrast, because the calculations do not explicitly include spin−orbit interactions, all calculations involving an asymptote including Pt^+ are referenced to the average energy of the spin−orbit components of the ^2D term at 0.418 eV.[65] A proper comparison between the experimental and calculated values must therefore include corrections for this different asymptotic energy,[35,36] as well as spin−orbit coupling in the molecular species as well. If it is assumed that spin−orbit coupling is largely quenched for all molecular species containing platinum (which may be reasonable as calculations indicate that PtO^+ ($^4\Sigma^-$) has a spin−orbit splitting of only 0.05 eV between the $\Omega = 3/2$ and 1/2 levels), then the theoretical values should be reduced by the 0.418 eV average energy. Such a simple correction is clearly an approximation and an overestimation. Nevertheless, given this 0.418 eV adjustment, the theoretical values calculated by Brönstrup et al.[24] are 3.09 (B3LYP/BS II), 2.96 (B3LYP/BS III), 2.95 (MR-QDPT/BS IV), and 2.92 (CASPT2/BS V) eV. These values are somewhat lower than our experimental BDE of 3.26 ± 0.07 eV, but certainly in reasonable agreement. Our own B3LYP calculations find a bond energy of 2.78 eV after correction.

4.2. Pt^+-C. PtC^+ is observed in the reaction of Pt^+ with CO. The bond dissociation energy is found to be $D_0(Pt^+-C)$ = 5.55 ± 0.05 eV. This value is in good agreement with values derived from related work in our laboratory, in which reactions of Pt^+ with CH_4, CD_4, C_2H_4, C_2D_4, and C_2H_2 were studied.[35,37] These reactions provide PtC^+ bond energies of 5.42 ± 0.15 (CH_4) and 5.41 ± 0.05 (CD_4),[35] 5.42 ± 0.05 (C_2H_4),[37] 5.45 ± 0.05 (C_2D_4),[37] 5.47 ± 0.06 (C_2H_2) eV,[37] respectively. The weighted average of all these values is 5.46 ± 0.05 eV (two standard deviations of the mean), taken as our best value.

Previously, we calculated BDEs for PtC^+ of 5.52 (HW), 5.43 (HW+), and 5.57 (HW+X) in good agreement with the experimental value. The calculations show that the ground state is $^2\Sigma^+$ and there is essentially a triple bond formed between the σ and π 5d(Pt) and 2p(C) orbitals.[35] The unpaired electron resides in a nonbonding orbital that is largely 6s(Pt) because the valence electron configuration of PtC^+ is $1\sigma^2 2\sigma^2 1\pi^4 1\delta^4 3\sigma^1$, where the character of the orbitals is comparable to those described above for PtO^+. Qualitatively, the relative bond energies of PtC^+ and PtO^+ can be understood by considering their bond order. Because PtC^+ does not occupy the 2π antibonding orbitals, whereas PtO^+ does, the bond order of PtC^+ is 3 and that of PtO^+ is 2 (presuming that the 3σ orbital is completely nonbonding). The ratio of the bond energies, 5.46 ± 0.05 eV and 3.26 ± 0.07 eV for PtC^+ and PtO^+, respectively, is 1.67 ± 0.05, which correlates well with their bond order ratio of 1.5.

4.3. Pt^+-CO. $PtCO^+$ is observed in the reaction of Pt^+ with CO_2. The bond dissociation energy is found to be $D_0(Pt^+-CO)$ = 2.28 ± 0.05 eV, which agrees well with the value of 2.20 ± 0.10 eV obtained from a previous CID experiment of Pt^+-CO with Xe.[38] The weighted average for the bond energy of Pt^+-CO is 2.26 ± 0.09 eV (two standard deviations of the mean). Theoretical calculations show that the ground state of $PtCO^+$ is $^2\Sigma^+$.[66] The bonding involves *sd*σ hybridization on Pt, covalent σ-donation and π-back-bonding, and electrostatic interactions, as discussed extensively elsewhere.[38,66] Theoretical calculations of Liang et al.[66] find a BDE of 2.33 eV (after adjustments described elsewhere),[38] whereas the present calculations yield 2.27 eV. Both values are in good agreement with the experimental values.

4.4. Pt^+-CO_2. The BDE of Pt^+-CO_2 is determined by CID of $PtCO_2^+$ with Ar and Xe. The CID thresholds are found to be 0.62 ± 0.05 eV for the Ar system and 0.76 ± 0.05 eV for the Xe system. Because the reproduction of the data is much better and competitive suppression of the CID channel from the ligand exchange reaction 16 is much less for the Ar system, the threshold value obtained from the Ar system should be a more accurate BDE for Pt^+-CO_2. This value is reasonably close to BDEs of Mg^+-CO_2 at 0.60 ± 0.06 eV,[59] V^+-CO_2 at 0.75 ± 0.04 eV,[10] Fe^+-CO_2 at 0.62 ± 0.04 eV,[60] and Mo^+-CO_2 at 0.51 ± 0.07 eV.[15] In the collisions of $PtCO_2^+$ with Ar/Xe, only simple CID and ligand exchange channels (reactions 15 and

TABLE 3: Bond Lengths (Å), Bond Angles (deg), and Energies Calculated at the B3LYP/HW+/6-311+G(3df) Level for $PtCO_2^+$

species	r(Pt−O)	r(Pt−C)	r(CO)	∠OPtC	∠OCO	∠PtOC	∠PtCO	E (h)	ZPE (h)	E_{rel} (eV)[a]
$Pt^+(^2D) + CO_2$			1.159		180.0			−307.397655	0.011722	0.000
$Pt^+(^4F) + CO_2$			1.159		180.0			−307.372604	0.011722	0.682
$PtO^+(^4\Sigma^-) + CO$	1.764		1.124					−307.304265	0.003790	2.330
$PtO^+(^2\Sigma^-) + CO$	1.766		1.124					−307.294324	0.003792	2.600
$PtCO^+(^2\Sigma^+) + O$		1.872	1.133					−307.289743	0.008017	2.838
$CPtO^+(^2A'') + O$	1.870	1.712		109.0				−307.060921	0.004107	8.960
$CPtO^+(^2A') + O$	1.942	1.695		104.2				−307.045749	0.003921	9.368
$Pt^+(CO_2)(^2\Sigma)TS$[b]	2.145		1.173, 1.141	0.0	180.0	180.0		−307.432497	0.012105	−0.938
$Pt^+(CO_2)(^2A')$	2.141		1.181, 1.139	13.0	177.5	142.9		−307.434303	0.012326	−0.981
$Pt^+(CO_2)(^2A'')$	2.145		1.181, 1.139	12.8	177.6	143.5		−307.434175	0.012280	−0.979
$Pt^+(CO_2)(^4\Delta)$	2.407		1.174, 1.142	0.0	180.0	180.0		−307.396401	0.012183	0.046
$Pt^+(CO_2)(^4\Sigma)$	2.517		1.177, 1.142	0.0	180.0	180.0		−307.383252	0.012196	0.405
$Pt^+(CO_2)(^4\Pi)$	2.539		1.175, 1.143	0.0	180.0	180.0		−307.380629	0.012151	0.475
$OPt^+(CO)(^4\Sigma^-,A'')$	1.804	2.069	1.113	180.0			180.0	−307.379854	0.009760	0.432
$OPt^+(CO)(^2\Sigma^-,A'')$	1.821	2.048	1.114	180.0			180.0	−307.372180	0.009780	0.641
$OPt^+(CO)(^2\Sigma-,A')$	1.850	2.038	1.116	180.0			180.0	−307.333064	0.010146	1.716
$OPt^+(CO)(^4\Sigma^-,A')$	1.896	2.038	1.115	180.0			180.0	−307.325205	0.009614	1.915
$OPt^+(CO)(^2A'')$	1.791	1.880	1.119	104.4			175.9	−307.375053	0.010069	0.571
$OPt^+(CO)(^2A')$	1.850	1.884	1.118	94.2			178.7	−307.356090	0.009933	1.083
$OPt^+(CO)(^2A'')TS$[b]	1.864	1.903	1.127, 1.792	56.8	132.3		167.2	-307.344860	0.009440	1.376
$OPt^+(CO)(^2A')TS$[b]	1.900	1.926	1.126, 1.775	55.3	130.6		167.8	-307.319019	0.008995	2.067
$OPt^+(CO)(^4A'')TS$[b]	2.253	1.951	1.129, 1.830	51.0	125.4		161.6	-307.285248	0.008102	2.962
$CPt^+O(^2A'')TS$[b]+O	1.964	1.745		71.2				-307.037016	0.003307	9.589
$CPt^+O(^2A')TS$[b]+O	1.970	1.729		67.3				-307.029898	0.003362	9.784

[a] Energies relative to the $Pt^+(^2D) + CO_2$ asymptote including corrections for zero-point energies (ZPE) scaled by 0.9804. These energies do not include the 0.418 eV adjustment for the spin−orbit levels of $Pt^+(^2D)$. [b] TS = transition state.

16) are found. No MO^+ species are observed at low energies, similar to previous work for other $M^+(CO_2)$ species,[10,15,59,60] These results show that $PtCO_2^+$ is an electrostatically bound adduct having an associative structure, $Pt^+ \cdot CO_2$.

Theoretical calculations find that the ground state of $Pt(CO_2)^+$ is $^2A'$ with a Pt^+-CO_2 BDE of 0.56 eV (after adjustment for the 0.418 eV atomic spin−orbit splitting energy), in reasonable agreement with experiment. The calculations find a $^2A''$ state lying only 0.002 eV higher in energy than the $^2A'$ ground state, such that definitive assignment of the ground state cannot be made. The geometries of these states are given in Table 3, where it can be seen that these species are not linear (Pt−O−C bond angles near 143°). The linear $^2\Sigma$ state is 0.04 eV higher than the ground state and has an imaginary frequency corresponding to a bending motion. A manifold of linear quartet states were also characterized, with the lowest being a $^4\Delta$ state lying 1.03 eV above the $^2A'$ ground state. A $^4\Sigma$ and $^4\Pi$ state lie 0.36 and 0.43 eV, respectively, higher in energy. The geometries of both the doublet and quartet states (Table 3) indicate that the CO_2 ligand is largely undistorted, indicating that the bonding must be largely electrostatic. However, there is a distinct change in the CO bond lengths such that the bond closer to Pt^+ elongates (by about 0.022 Å for the doublet states and 0.016 Å for the quartet states), whereas that farther away contracts (by 0.020 Å for the doublet states and 0.017 Å for the quartet states) such that it is midway between the bond lengths for free CO and CO_2 (Table 3).

4.5. OPt^+-CO. In the following paper,[67] $PtCO_2^+$ is also observed as a product in the reaction of PtO^+ with CO_2 and identified as having a OPt^+-CO structure. The thermochemistry measured there indicates that $D_0(OPt^+-CO) = 2.21 \pm 0.10$ eV, similar to the bond energy of Pt^+-CO, 2.26 ± 0.09 eV.[38] Our calculations indicate that the inserted $OPtCO^+$ species has several stable minima as detailed in Table 3. The ground state is calculated to be $^4\Sigma^-$ ($^4A''$ in C_s symmetry) with a OPt^+-CO BDE of 1.90 eV, in reasonable agreement with experiment. Other linear states of the inserted $OPtCO^+$ species were also characterized and include a $^2\Sigma^-$ ($^2A''$), $^2\Sigma^-$ ($^2A'$), and a $^4\Sigma^-$ ($^4A'$) lying 0.21, 1.28, and 1.48 eV, respectively, above the $^4\Sigma^-$ ground state. In all of these linear states, the Pt−O bond length is elongated compared to $PtO^+(^4\Sigma^-)$ by between 0.040 and 0.13 Å. Likewise, the Pt−C bond length is longer than in $PtCO^+(^2\Sigma^+)$ by 0.17 to 0.20 Å, and interestingly, the CO bond distance decreases slightly, even compared to free CO. Accompanying these changes, the CO stretching frequency increases: values calculated here are about 2300 cm^{-1} for all four states of OPt^+-CO vs an experimental value of 2205 cm^{-1} and a theoretical value of 2262 cm^{-1} for $PtCO^+$.[66] Bent states of $OPtCO^+$ were also identified as stable minima on the $^2A''$ and $^2A'$ surfaces. These have OPtC bond angles of 104° and 94°, respectively, and Pt−C bond lengths comparable to $PtCO^+(^2\Sigma^+)$. These $^2A''$ and $^2A'$ bent states of $OPtCO^+$ lie 0.14 and 0.65 eV, respectively, above the $^4\Sigma^-$ ground state.

5. Discussion

5.1. Periodic Trends in Thermochemistry of Metal Oxides. The bond energies and ionization energies of platinum and platinum monoxide can be related according to the thermochemical cycle, $D(M-O) + IE(M) = D(M^+-O) + IE(MO)$.[12] The neutral PtO BDE has been measured as 3.82 ± 0.24 eV using the mass spectrometric Knudsen cell method.[44,63,64] Thus, given IE(Pt) = 8.95868 ± 0.00011 eV[56] and the PtO^+ BDE measured here, we can calculate that IE(PtO) is 9.52 ± 0.25 eV. This is close to the lower limit for IE(PtO) of 10.1 ± 0.3 eV determined by electron impact studies in the early literature.[63] Thus, ionization of PtO reduces the bond strength (or equivalently, oxidation raises the ionization energy) by 0.56 ± 0.25 eV. Similar behavior is also observed for NiO^+ and PdO^+, the first-row and second-row congeners of platinum monoxide.[12]

The electron configuration of PtO is $1\sigma^2 2\sigma^2 1\pi^4 1\delta^4 2\pi^2 3\sigma^2$, giving a $^3\Sigma^-$ ground state,[22] in contrast to the $^1\Sigma^+$ ground state assigned in the early literature.[44] In this picture, the decrease in bond energy upon ionization appears to suggest that the 3σ orbital has bonding character, but the dichotomy is that removal of this electron is favored over removing an electron from a 2π antibonding orbital.[22] This is probably a result of the favorable spin exchange energy for the $^4\Sigma^-$ state of PtO^+ because the

first three excited states are calculated as $^2\Sigma^-(2\pi^2 3\sigma^1)$ at 0.51 eV, $^2\Pi(2\pi^3 3\sigma^0)$ at 0.83 eV, and $^2\Delta(2\pi^2 3\sigma^1)$ at 0.92 eV. Removal of an electron from the 2π antibonding orbital yields states that were not included in previous calculations.[22]

An alternative way of viewing platinum monoxide is in terms of ionic bonding,[68,69] in which Pt can be regarded as a monopositive cation, Pt^+, bound to the O^- anion. As pointed out by Siegbahn,[69] because the neutral metal oxides have high spin states, $O^-(^2P)$ must couple with a high spin state of Pt^+, which necessitates promotion to a $^4F(6s^15d^8)$ configuration from the $^2D(5d^9)$ ground state. The promotion energy is calculated as the average of the excitation energies of the high- and low-spin coupled $6s^15d^8$ states, $E_p(Pt^+) = 1.85$ eV.[65] The same promotion energy is required to couple Pt^+ and O to diabatically form PtO^+ in its $^4\Sigma^-$ ground state. Thus the ionic PtO^+ BDE is lower than that of neutral PtO because the negative charge on the oxygen is smaller leading to a smaller ionic interaction (formally, bonding of Pt^+ with O vs Pt^+ with O^-).

The difference between the neutral and ionic BDEs is smaller for the platinum monoxide systems (0.56 eV) than that for the palladium monoxide (1.38 eV)[12] or nickel monoxide (1.17 eV)[6,70] systems. On the basis of the discussion above, this observation suggests that the third-row metal monoxide has less ionic character. Similar to the M^+-H species,[36] this probably results from efficient 6s-5d hybridization on Pt, a result of lanthanide contraction and relativistic effects, which facilitate covalent bonding in the third-row metal monoxide.

Compared with the $Pd^+ + O_2$ reaction system,[12] the cross section for reaction 2 is a little larger. This is because the platinum system has a lower threshold (1.85 eV) than the palladium system (3.66 eV). Compared with the $Ni^+ + O_2$ reaction system,[6] the cross section of PtO^+ is slightly less than that of NiO^+ (maxima of 2.2 vs 2.5 $\times$ 10^{-16} cm^2). This is consistent with the more comparable threshold energies (1.85 vs 2.38 eV), although the lower threshold for Pt^+ might have been anticipated to lead to a larger cross section. The differences may lie in the details of the reactant states, $^2D_{5/2}$ for Pt^+ vs a thermally populated distribution of $^2D_{5/2}$ and $^2D_{3/2}$ states at 2200 K for Ni^+.

The magnitudes of the reaction cross sections for Pt^+ systems are the largest for O_2, followed by CO_2, with CO being the smallest. This correlates with the bond energies of O_2 at 5.12 eV, CO_2 at 5.45 eV, and CO at 11.11 eV.

5.2. Reaction of $PtO^+ + CO$. We also observe $PtCO^+$ in the reaction of $PtO^+ + CO$. Given the bond energies for PtO^+ and $PtCO^+$ determined above from multiple sources, this ligand exchange reaction should be endothermic by 1.00 $\pm$ 0.11 eV. (Indeed, this difference can be seen directly in the relative thresholds for formation of $PtO^+ + CO$ and $PtCO^+ + O$ in the $Pt^+ + CO_2$ reaction system, Table 2.) Instead we measure a much smaller threshold of 0.35 $\pm$ 0.05 eV (Table 2). Although we tried to introduce CO into the FT source to quench excited states of PtO^+ to no effect, this threshold difference of 0.65 $\pm$ 0.12 eV can plausibly be assigned to such excited states for the following reasons. (1) The BDE of 3.26 $\pm$ 0.07 eV for Pt^+-O determined from the O_2, CO, and CO_2 reaction systems should be for the ground electronic state of PtO^+. (This conclusion is also confirmed by studies of the nearly thermoneutral forward and reverse reactions: $Pt^+ + NO_2 \leftrightarrow PtO^+ + NO$ where $D_0(O-NO) = 3.116$ eV.[37]) Likewise the BDE of 2.26 $\pm$ 0.09 eV for $PtCO^+$ as determined from two independent sources should refer to the ground electronic state of this ion. Good agreement of this thermochemistry with theoretical calculations bolsters these conclusions. Therefore, it seems very unlikely that the PtO^+ BDE could be as low as 2.56 eV or that the $PtCO^+$ BDE could be as high as 2.96 eV. (2) The ligand exchange product $PtCO^+$ formed in reaction 14 must be in its ground electronic state because production of excited $PtCO^+$ would have a higher threshold (>1.00 $\pm$ 0.11 eV). (3) The threshold discrepancy of 0.65 $\pm$ 0.12 eV is close to the difference of 0.51 eV calculated as the excitation energy from the $^4\Sigma^-$ ground state to the $^2\Sigma^-$ first excited state of PtO^+.[22] (4) As noted above, the cross section for $PtCO^+$ formation in Figure 5 exhibits a second feature that becomes obvious near 2 eV and can be assigned to the reaction of $PtO^+(^4\Sigma^-)$. Depending on the analysis used for the lower energy feature, the apparent threshold for this second feature can vary appreciably, but the analysis shown in Figure 5 yields a value of 1.08 $\pm$ 0.10 eV, within experimental error of the value expected, 1.00 $\pm$ 0.11 eV. (5) Alternate explanations for the low threshold, such as formation of $C-Pt^+-O$, cannot be correct as formation of such a species should have an even higher threshold. Compared to $PtCO^+$, this inserted species is estimated to lie 4.65 eV higher in energy according to bond additivity and 6.12 eV higher according to our calculations (Table 3). (6) The fraction of PtO^+ excited state in the beam may be quite small. Other reactions of PtO^+, discussed fully in the following paper,[67] exhibit no obvious signs of excited states except for the $PtO^+ + O_2$ reaction. In these processes, the magnitude of any reactivity attributable to excited states is certainly no more than a few percent of the dominant reaction observed. This suggests that the reactivity of CO with $PtO^+(^2\Sigma^-)$ is much higher than with $PtO^+(^4\Sigma^-)$, as discussed further in the next section and in the following paper.[67]

Potential Energy Surfaces and Reaction Mechanisms. Our experiments can probe the potential energy surfaces (PESs) for the activation of small molecules by Pt^+ by independently starting at three separate places on the same global surface, i.e., reactants, intermediates, and products. The PES for the PtO_2^+ system is discussed in detail in the following paper.[67] Here we focus on the CO_2 and CO systems.

For the activation of CO_2 by $Pt^+(^2D)$, the first step is to form an associative complex of $Pt^+ \cdot OCO$ with a nonlinear, end-on structure at -0.62 ± 0.05 eV. The present calculations indicate that formation of this adduct can occur on both $^2A''$ and $^2A'$ surfaces, Figure 6. Observation of both PtO^+ and $PtCO^+$ suggests the subsequent formation of the dissociative/insertion complex, $O-Pt^+-CO$. The energy of such an intermediate is close to that of the entrance channel of $Pt^+ + CO_2$ on the basis of bond additivity, whereas calculations (Table 3) indicate that the energy is 0.43 eV higher than the reactant asymptote (0.85 eV if the 0.418 eV adjustment for the spin–orbit levels of Pt^+ is included). $PtO^+(^4\Sigma^-) + CO(^1\Sigma^+)$ and $PtCO^+(^2\Sigma^+) + O(^3P)$ are then formed with endothermicities of 2.19 $\pm$ 0.07 and 3.17 $\pm$ 0.05 eV relative to the entrance channel of $Pt^+(^2D) + CO_2(^1\Sigma_g^+)$. Note that $Pt^+(^2D) + CO_2(^1\Sigma_g^+)$ can form $PtCO^+(^2\Sigma^+) + O(^3P)$ in a spin-allowed process, whereas formation of the $PtO^+(^4\Sigma^-) + CO(^1\Sigma^+)$ ground state is spin-forbidden, but that of excited-state $PtO^+(^2\Sigma^-) + CO(^1\Sigma^+)$ is spin-allowed. (In the following discussion, it should be realized that platinum is sufficiently heavy that spin may no longer be a good quantum number. In this context, it may be more appropriate to think of spin-allowed and spin-forbidden processes as being diabatically favored and disfavored, respectively. In any case, alternate explanations for some of the phenomena observed are not apparent.)

One can anticipate that the putative $O-Pt^+-CO$ intermediate is likely to have a quartet spin ground state given that the $^4\Sigma^-$ and $^2\Sigma^-$ states of PtO^+ have the same electronic configuration[22]

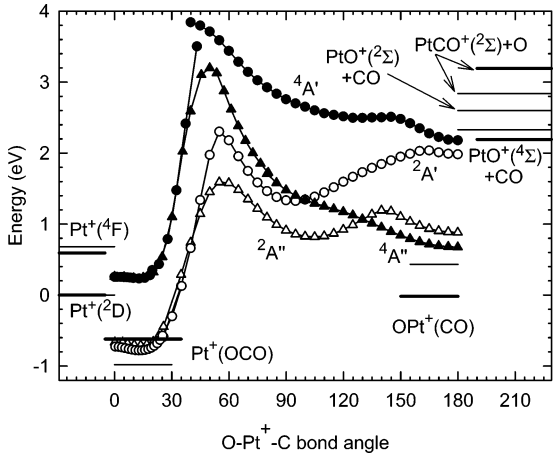

Figure 6. Relaxed potential energy surface scans of the bond angle in the $PtCO_2^+$ system calculated at the B3LYP/HW+/6-31+G(2d) level. Circles and triangles represent surfaces of A′ and A″ symmetry, respectively. Open and closed symbols represent doublet and quartet surfaces, respectively. Calculated energies (B3LYP/HW+/6-311+G(3df) level) of reactant ($Pt^+ + CO_2$), intermediates, and product asymptotes are indicated by horizontal bars to the left and right, respectively. Thicker horizontal bars indicate experimental energies of reactants, intermediates, and products.

and should therefore interact with CO similarly. Our calculations confirm that this is true as can be seen by the relative energies of the $^4\Sigma^-(^4A'')$ and $^2\Sigma^-(^2A'')$ surfaces for linear OPt^+-CO (Table 3, Figure 6). Interestingly, the $^2A''$ surface has another potential well as the CO molecule approaches $PtO^+(^2\Sigma^-)$ from the side, presumably because the low spin state allows an appropriate acceptor orbital (possibly the 2π or 3σ) to be empty, whereas this cannot occur for the high spin state. In any case, the $^4A''$ and $^2A''$ intermediates correlate with formation of $PtO^+(^4\Sigma^-) + CO(^1\Sigma^+)$ and $PtO^+(^2\Sigma^-) + CO(^1\Sigma^+)$, respectively. Therefore, formation of PtO^+ at its thermodynamic threshold must involve a potential energy surface crossing from the doublet surface of the ground state reactants to a quartet surface that diabatically correlates with excited $Pt^+(^4F) + CO_2(^1\Sigma_g^+)$. The potential energy surfaces calculated here suggest that this surface crossing probably occurs in the vicinity of the OPt^+-CO intermediate. This also seems probable because the barrier to formation of this inserted intermediate is lowest on the $^2A''$ surface, which evolves from ground-state reactants. At higher energies, the spin-allowed formation of PtO^+ in excited doublet states can probably also occur. The possibility of having both a spin-forbidden pathway to form $PtO^+(^4\Sigma^-)$ and a spin-allowed pathway forming $PtO^+(^2\Sigma^-)$ may explain the complex energy dependence of the PtO^+ cross section (Figure 4) and why competition with spin-allowed formation of $PtCO^+$ is so severe. Similar phenomena also are found in the $V^+ + CO_2$ and $V^+ + CS_2$ reaction systems.[10,71]

The experimental observation that the thresholds for formation of PtO^+ and $PtCO^+$ in reactions 4 and 5 agrees with other thermodynamic information indicates that there are no barriers in excess of the endothermicity of the reactions along the reaction paths. This is in agreement with the calculated potential energy surfaces, Figure 6. The height of the barrier along the $^2A''$ surface is the lowest and is calculated to lie 1.376 eV above the energy of the reactants (Table 3). This is 0.954 eV below the energy of the $PtO^+(^4\Sigma^-) + CO(^1\Sigma^+)$ product asymptote. The barrier on the $^2A'$ surface is calculated to lie at energies 2.067 and 0.263 eV, respectively, whereas that along the $^4A''$ surface is found at 2.962 above the reactants asymptote and lies 0.632 eV above the product asymptote, as qualitatively shown in Figure 6. (The energies relative to the $Pt^+ + CO_2$ asymptote ignore the 0.418 eV adjustment for the spin−orbit states of Pt^+.) The $^4A'$ surface lies higher than the other three characterized here. It closely matches the $^4A''$ surface for small $O-Pt^+-C$ bond angles (Figure 6), but lies considerably higher in energy at angles larger than the transition state. The latter was never clearly identified but must lie at a geometry similar to the transition state on the $^4A''$ surface. As this surface must be relatively unimportant under experimental conditions, further characterization of the transition state was not pursued.

For the reaction of $PtO^+(^4\Sigma^-)$ with $CO(^1\Sigma^+)$, production of $Pt^+(^2D) + CO_2(^1\Sigma_g^+)$, the reverse process of CO_2 activation by Pt^+, is exothermic by 2.19 ± 0.07 eV, but spin-forbidden. There are spin-allowed channels that yield $Pt^+(^4F_J) + CO_2(^1\Sigma_g^+)$, 0.59, 1.16, 1.65, and 1.96 eV for $J = 9/2$, 7/2, 5/2, and 3/2,[72] respectively, higher in energy than the $Pt^+(^2D_{5/2})$ ground state but formation of all of these states is also exothermic, by 1.60, 1.03, 0.54, and 0.23 eV, respectively. A likely possibility is that the large exothermic feature in the Pt^+ cross section, Figure 5, comes from the spin-forbidden process, whereas the feature beginning near 1 eV can be attributed to the spin-allowed process. Clearly, the observation that this reaction is exothermic and efficient suggests that the rearrangements necessary to form CO_2 after CO binds with PtO^+ are not inhibited by the transition state involved, i.e., the energy barriers are below the asymptote of $PtO^+(^4\Sigma^-) + CO(^1\Sigma^+)$ reactants, in agreement with the calculated surfaces, Figure 6. However, the spin-allowed processes that occur along the $^4A''$ surface must surmount a barrier calculated to lie 0.63 eV *above* the $PtO^+(^4\Sigma^-) + CO(^1\Sigma^+)$ reactants (Table 3), in reasonable agreement with the onset of the endothermic feature in the Pt^+ cross section of Figure 5.

The ligand exchange reaction leading to $PtCO^+(^2\Sigma^+) + O(^3P)$ must occur via the $O-Pt^+-CO$ intermediate and has an endothermicity of 1.00 ± 0.11 eV relative to the entrance channel of $PtO^+(^4\Sigma^-) + CO(^1\Sigma^+)$. We believe that this reaction corresponds to the second feature for the production of $PtCO^+$ in Figure 5, which rises slowly from its threshold because it competes strongly with both spin-allowed and spin-forbidden eliminations of CO_2, which are both thermodynamically more favorable. As discussed above, the low energy feature in the $PtCO^+$ cross section, Figure 5, is attributed to the reaction of $PtO^+(^2\Sigma^-) + CO(^1\Sigma^+)$. We believe that this reaction is very sensitive to the presence of small amounts of the $PtO^+(^2\Sigma^-)$ excited state, which can be rationalized as follows. In the $PtO^+ + CO$ reaction, reaction of ground-state $PtO^+(^4\Sigma^-)$ with $CO(^1\Sigma_g^+)$ will initially evolve along a quartet surface, and thus can form the $^4A''$ ground state of $OPt^+(CO)$. Similarly, reaction of excited $PtO^+(^2\Sigma^-)$ with $CO(^1\Sigma_g^+)$ will form the $^2A''$ excited state of $OPt^+(CO)$. On the basis of calculated potential energy surfaces (Figure 6), we note that reaction of CO with $PtO^+(^4\Sigma^-)$ strongly favors a collinear approach of C toward the Pt end of the molecule, thereby constraining favorable geometries for this interaction. In contrast, reaction of CO with $PtO^+(^2\Sigma^-)$ has a favorable approach both collinearly and from the side, making this interaction much less constrained dynamically. Now consider the interaction of $O(^3P)$ with $PtCO^+(^2\Sigma^+)$, where the most attractive surface, which would involve covalent bond formation, evolves along a doublet surface to form the $^2A''$ excited state of $OPt^+(CO)$. The $O(^3P) + PtCO^+(^2\Sigma^+)$ species can also interact along a quartet surface, although this does not obviously involve covalent bond formation. This may suggest that this quartet surface is inhibited in some manner, although calculations (B3LYP/HW-ECP/6-31+G(2d)) of the

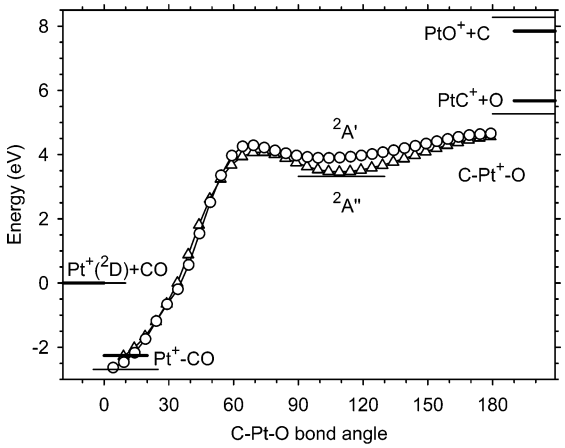

Figure 7. Relaxed potential energy surface scans of the bond angle in the $PtCO^+$ system calculated at the B3LYP/HW+/6-31+G(2d) level. Circles and triangles represent surfaces of A′ and A″ symmetry, respectively. Calculated energies (B3LYP/HW+/6-311+G(3df) level) of reactant (Pt^+ + CO) and product asymptotes are indicated by horizontal bars to the left and right, respectively. Thicker horizontal bars indicate experimental energies of reactants, intermediates, and products.

quartet and doublet surfaces for dissociation of the $^4A''$ and $^2A''$ states of $OPt^+(CO)$ show smooth, monotonic evolution to the $PtO^+(^4\Sigma^-,^2\Sigma^-)$ + CO and $PtCO^+$ $(^2\Sigma^+)$ + O products. It should also be kept in mind that these dissociations compete with the thermodynamically favored elimination of CO_2 along both spin-allowed and spin-forbidden paths, although CO_2 elimination is entropically disfavored because of the large barrier. Apparently, the dynamics for the production of $PtCO^+$ + O is facile in the reaction of CO with the $PtO^+(^2\Sigma^-)$ excited state and thus competes well with CO_2 elimination, but the collinear approach required for the reaction involving the $PtO^+(^4\Sigma^-)$ ground-state inhibits this channel. Thus, the presence of the $PtO^+(^2\Sigma^-)$ excited states is evident in this reaction system, whereas it is not obvious in the other reactions of PtO^+, as studied in the following paper.[67]

For the activation of $CO(^1\Sigma^+)$ by $Pt^+(^2D)$, the first step is to form a $PtCO^+(^2\Sigma^+)$ intermediate having a linear, end-on structure at 2.26 ± 0.09 eV below the reactants. The observation of both PtC^+ and PtO^+ products suggests that activation of the CO bond has occurred to form $C-Pt^+-O$, which has an energy of ~2.4 eV (based on bond additivity) above the entrance channel of Pt^+ + CO. Calculations indicate that the $CPtO^+$ species has a $^2A''$ ground state that lies in a shallow well 3.431 eV above the reactants, Figure 7. Thus, the calculations indicate that the strong PtC^+ and PtO^+ bonds are stronger than the analogues in $CPtO^+$, a result that is not surprising as electron density must be shared in the two ligand complex. An excited $^2A'$ state was also found lying 0.41 eV higher in energy. Note that the Pt−O bond is shorter in the $^2A''$ state than in the $^2A'$ state, whereas the order switches for the Pt−C bond length (Table 3). PtC^+ + O and PtO^+ + C products can be formed from the $C-Pt^+-O$ and have endothermicities of 5.56 ± 0.05 eV and 7.84 ± 0.05 eV, respectively, relative to the entrance channel of Pt^+ + CO. The agreement of the thresholds measured for these two channels with other thermodynamic information indicates that there are no barriers along the reaction paths in excess of the endothermicity of the reactions, in agreement with the calculated potential energy surface. The transition states on the $^2A''$ and $^2A'$ surfaces were calculated to lie 3.979 and 4.174 eV, respectively, above the reactant asymptote, Table 3. (The energies relative to the Pt^+ + CO asymptote ignore the 0.418 eV adjustment for the spin−orbit states of Pt^+.) The reactions $Pt^+(^2D)$ + $CO(^1\Sigma^+)$ → $PtO^+(^4\Sigma^-)$ + $C(^3P)$ and → $PtC^+(^2\Sigma^+)$ + $O(^3P)$ are both spin-allowed.

6. Conclusion

Guided ion beam tandem mass spectrometry is used to characterize the kinetic energy dependences of the reactions of Pt^+ with O_2, CO, and CO_2, PtO^+ + CO, and collision-induced dissociation of $PtCO_2^+$ with Xe and Ar. Analyses of endothermic reaction cross sections lead to 0 K bond dissociation energies for Pt^+-O, Pt^+-C, Pt^+-CO, and Pt^+-CO_2, which are reasonably consistent with available theoretical values. These results are used to construct potential energy surfaces for the activation of CO_2 and CO by Pt^+. This helps elucidate the reaction mechanisms, which are found to involve bond insertion processes and for CO_2, coupling between surfaces of different spin.

Acknowledgment. This work was supported by the National Science Foundation under Grant CHE-0135517. X.-G. Zhang thanks R. Liyanage for technical help with the experiments. The authors thank R. B. Metz for supplying the bond energy of PtO^+ from his photodissociation experiment, and J. N. Harvey and D. Schröder for supplying details about their calculations of PtO^+.

Supporting Information Available: Three figures showing data for the reaction of Pt^+ with CO_2 and $PtCO_2^+$ with Xe and Ar. This material is available free of charge via the Internet at http://pubs.acs.org.

References and Notes

(1) Somorjai, G. A. *Introduction to Surface Chemistry and Catalysis*; Wiley: New York, 1994.
(2) Crabtree, R. H. *The Organometallic Chemistry of the Transition Metals*, 2nd ed.; Wiley: New York, 1994.
(3) Aristov, N.; Armentrout, P. B. *J. Phys. Chem.* **1986**, *90*, 5135.
(4) Loh, S. K.; Fisher E. R.; Lian, L.; Schultz, R. H.; Armentrout, P. B. *J. Phys. Chem.* **1989**, *93*, 3159.
(5) Loh, S. K.; Lian, L.; Armentrout, P. B. *J. Chem. Phys.* **1989**, *91*, 6148.
(6) Fisher E. R.; Elkind, J. L.; Clemmer, D. E.; Georgiadis, R.; Loh, S. K.; Aristov, N.; Sunderlin, L. S.; Armentrout, P. B. *J. Chem. Phys.* **1990**, *93*, 2676.
(7) Clemmer, D. E.; Elkind, J. L.; Aristov, N.; Armentrout, P. B. *J. Chem. Phys.* **1991**, *95*, 3387.
(8) Clemmer, D. E.; Dalleska, N. F.; Armentrout, P. B. *J. Chem. Phys.* **1991**, *95*, 7263.
(9) Clemmer, D. E.; Dalleska, N. F.; Armentrout, P. B. *Chem. Phys. Lett.* **1992**, *190*, 259.
(10) Sievers, M. R.; Armentrout, P. B. *J. Chem. Phys.* **1995**, *102*, 754.
(11) Rodgers, M. T.; Walker, B.; Armentrout, P. B. *Int. J. Mass Spectrom.* **1999**, *182*−*183*, 99.
(12) Chen, Y.-M.; Armentrout, P. B. *J. Chem. Phys.* **1995**, *103*, 618.
(13) Sievers, M. R.; Chen, Y.-M.; Armentrout, P. B. *J. Chem. Phys.* **1996**, *105*, 6322.
(14) Sievers, M. R.; Armentrout, P. B. *Int. J. Mass Spectrom.* **1998**, *179*−*180*, 103.
(15) Sievers, M. R.; Armentrout, P. B. *J. Phys. Chem. A* **1998**, *102*, 10754.
(16) Sievers, M. R.; Armentrout, P. B. *Inorg. Chem. A* **1999**, *38*, 397.
(17) Sievers, M. R.; Armentrout, P. B. *Int. J. Mass Spectrom.* **1999**, *185*−*187*, 117.
(18) Weber, M. E.; Elkind, J. L.; Armentrout, P. B. *J. Chem. Phys.* **1986**, *84*, 1521.
(19) Clemmer, D. E.; Weber, M. E.; Armentrout, P. B. *J. Phys. Chem.* **1992**, *96*, 10888.
(20) Dalleska, N. F.; Armentrout, P. B. *Int. J. Mass Spectrom. Ion Processes* **1994**, *134*, 203.
(21) Wesendrup, R.; Schröder, D.; Schwarz, H. *Angew. Chem., Int. Ed. Engl.* **1994**, *33*, 1174.
(22) Heinemann, C.; Koch, W.; Schwarz, H. *Chem. Phys. Lett.* **1995**, *245*, 509.

(23) Pavlov, M.; Blomberg, M. R. A.; Siegbahn, P. E. M.; Wesendrup, R.; Heinemann, C.; Schwarz, H. *J. Phys. Chem. A* **1997**, *101*, 1567.
(24) Brönstrup, M.; Schröder, D.; Kretzschmar I.; Schwarz, H.; Harvey, J. N. *J. Am. Chem. Soc.* **2001**, *123*, 142.
(25) Schröder, D.; Schwarz, H. *Angew. Chem., Int. Ed. Engl.* **1995**, *34*, 1973.
(26) Armentrout, P. B.; Kickel, B. L. In *Organometallic Ion Chemistry*; Freiser, B. S., Ed.; Kluwer: Dordrecht, 1996; p 1.
(27) Armentrout, P. B. In *Topics in Organometallic Chemistry*; Brown, J. M., Hofmann, P., Eds.; Springer-Verlag: Berlin, 1999; Vol. 4-I, p 1.
(28) Kretzschmar, I.; Schröder, D.; Schwarz, H.; Armentrout, P. B. *Adv. Met. Semicond. Clusters* **2001**, *5*, 347.
(29) Loh, S. K.; Hales, D. A.; Lian, L.; Armentrout, P. B. *J. Chem. Phys.* **1989**, *90*, 5466.
(30) Schultz, R. H.; Armentrout, P. B. *Int. J. Mass Spectrom. Ion Processess* **1991**, *107*, 29.
(31) Teloy, E.; Gerlich, D. *Chem. Phys.* **1974**, *4*, 417.
(32) Gerlich, D. *Adv. Chem. Phys.* **1992**, *82*, 1.
(33) Ervin, K. M.; Armentrout, P. B. *J. Chem. Phys.* **1985**, *83*, 166.
(34) Chantry, P. J. *J. Chem. Phys.* **1971**, *55*, 2746.
(35) Zhang, X.-G.; Liyanage, R.; Armentrout, P. B. *J. Am. Chem. Soc.* **2001**, *123*, 5563.
(36) Zhang, X.-G.; Armentrout, P. B. *J. Chem. Phys.* **2002**, *116*, 5565.
(37) Zhang, X.-G.; Armentrout, P. B. Work in progress.
(38) Zhang, X.-G.; Armentrout, P. B. *Organometallics* **2001**, *20*, 4266.
(39) Armentrout, P. B. *Int. J. Mass Spectrom.* **2000**, *200*, 219.
(40) Chesnavich, W. J.; Bowers, M. T. *J. Phys. Chem.* **1979**, *83*, 900.
(41) Armentrout, P. B. *Adv. Gas-Phase Ion Chem.* **1992**, *1*, 83.
(42) Muntean, F.; Armentrout, P. B. *J. Chem. Phys.* **2001**, *115*, 1213.
(43) Armentrout, P. B. *Int. J. Mass Spectrom.* **2000**, *200*, 219.
(44) Huber, K. P.; Herzberg, G. *Molecular Spectra and Molecular Structure*; IV. Constants of Diatomic Molecules. Van Nostrand Reinhold: New York, 1979.
(45) Shimanouchi, T. *Tables of Molecular Vibrational Frequencies*; Consolidated Vol. I, NSRDS-NBS *39*, 1972.
(46) The vibrational frequency of PtO^+ is taken from the theoretical value of 799 cm^{-1} (ref 24).
(47) Becke, A. D. *J. Chem. Phys.* **1993**, *98*, 5648.
(48) Lee, C.; Yang, W.; Parr, R. G. *Phys. Rev. B* **1988**, *37*, 785.
(49) Frisch, M. J.; Trucks, G. W.; Schlegel, H. B.; Scuseria, G. E.; Robb, M. A.; Cheeseman, J. R.; Zakrzewski, V. G.; Montgomery, J. A., Jr.; Stratmann, R. E.; Burant, J. C.; Dapprich, S.; Millam, J. M.; Daniels, A. D.; Kudin, K. N.; Strain, M. C.; Farkas, O.; Tomasi, J.; Barone, V.; Cossi, M.; Cammi, R.; Mennucci, B.; Pomelli, C.; Adamo, C.; Clifford, S.; Ochterski, J.; Petersson, G. A.; Ayala, P. Y.; Cui, Q.; Morokuma, K.; Malick, D. K.; Rabuck, A. D.; Raghavachari, K.; Foresman, J. B.; Cioslowski, J.; Ortiz, J. V.; Baboul, A. G.; Stefanov, B. B.; Liu, G.; Liashenko, A.; Piskorz, P.; Komaromi, I.; Gomperts, R.; Martin, R. L.; Fox, D. J.; Keith, T.; Al-Laham, M. A.; Peng, C. Y.; Nanayakkara, A.; Gonzalez, C.; Challacombe, M.; Gill, P. M. W.; Johnson, B.; Chen, W.; Wong, M. W.; Andres, J. L.; Gonzalez, C.; Head-Gordon, M.; Replogle, E. S.; Pople, J. A. *Gaussian 98*, Revision A.11; Gaussian, Inc.: Pittsburgh, PA, 1998.
(50) Ohanessian, G.; Brusich, M. J.; Goddard, W. A., III. *J. Am. Chem. Soc.* **1990**, *112*, 7179.
(51) Hay, P. J.; Wadt, W. R. *J. Chem. Phys.* **1985**, *82*, 299.
(52) Foresman, J. B.; Frisch, A. E. *Exploring Chemistry with Electronic Structure Methods*; Gaussian, Inc.: Pittsburgh, PA, 1996.
(53) Lias, S. G.; Bartmess, J. E.; Liebman, J. F.; Holmes, J. L.; Levin, R. D.; Mallard, W. G. *J. Phys. Chem. Ref. Data, Suppl. 1*, **1988**.
(54) Gioumousis, G.; Stevenson, D. P. *J. Chem. Phys.* **1958**, *29*, 294.
(55) Tonkyn, R. G.; Winniczek, J. W.; White, M. G. *Chem. Phys. Lett.* **1989**, *164*, 137.
(56) Marijnissen, A.; Meulen, J. J.; Hackett, P. A.; Simard, B. *Phys. Rev. A* **1995**, *52*, 2606.
(57) Wang, L.; Reutt, J. E.; Lee, Y. T.; Shirley D. A. *J. Electron Spectrosc. Relat. Phenom.* **1988**, *47*, 167.
(58) Erman, P.; Karawajczyk, A.; Rachlew-Kallne, E.; Stromhalm, C.; Larsson, J.; Persson, A.; Zerne, R. *Chem. Phys. Lett.* **1993**, *215*, 173.
(59) Andersen A.; Muntean F.; Walter, D.; Rue, C.; Armentrout P. B. *J. Phys. Chem. A* **2000**, *104*, 692.
(60) Tjelta, B. L.; Walter, D.; Armentrout P. B. *Int. J. Mass Spectrom.* **2001**, *204*, 7.
(61) Armentrout, P. B.; Simons, J. *J. Am. Chem. Soc.* **1992**, *114*, 8627.
(62) Thompson, C. J.; Stringer, K. L.; McWilliams, M.; Metz, R. B. *Chem. Phys. Lett.* **2003**, *376*, 588.
(63) Norman, J. H.; Staley, H. G.; Bell, W. E. *J. Phys. Chem.* **1967**, *71*, 3686.
(64) Norman, J. H.; Staley, H. G.; Bell, W. E. *Adv. Chem. Series* **1968**, *71*, 101.
(65) Moore, C. E. *Atomic Energy Levels*, NSRDS-NBS, 1971, 35/Vol. III.
(66) Liang, B.; Zhou, M.; Andrews, L. *J. Phys. Chem. A* **2000**, *104*, 3905.
(67) Zhang, X.-G.; Armentrout, P. B. *J. Phys. Chem. A* **2003**, *107*, 8915.
(68) Langhoff, S. R.; Bauschlicher, C. W., Jr. *J. Chem. Phys.* **1988**, *89*, 2160.
(69) Siegbahn, P. E. M. *Chem. Phys. Lett.* **1993**, *201*, 15.
(70) Pedley, J. B.; Marshall, E. M. *J. Phys. Chem. Ref. Data* **1983**, *12*, 967.
(71) Rue, C.; Armentrout, P. B.; Kretzschmar I.; Schröder, D.; Harvey, J. N.; Schwarz, H. *J. Chem. Phys.* **1999**, *110*, 7858.
(72) Sievers, M. R.; Chen, Y.-M.; Armentrout, P. B. *J. Phys. Chem.* **1996**, *100*, 54.